MODELING THE ORIGIN OF THE ORIENTALE BASIN MASCON. David M. Blair[1], Brandon C. Johnson[1], Andrew M. Freed[1], H. Jay Melosh[1], Gregory A. Neumann[2], Sean C. Solomon[3,4], and Maria T. Zuber[5]; [1]Department of Earth and Atmospheric Sciences, Purdue University, West Lafayette, IN, USA, dblair@purdue.edu; [2]NASA Goddard Space Flight Center, Greenbelt, MD 20771, USA; [3]Department of Terrestrial Magnetism, Carnegie Institution of Washington, Washington, DC 20015, USA; [4]Lamont-Doherty Earth Observatory, Columbia University, Palisades, NY 10974; [5]Department of Earth, Atmospheric and Planetary Sciences, Massachusetts Institute of Technology, Cambridge, MA 02139, USA.

Introduction: Positive gravity anomalies in large lunar basins—mass concentrations, or "mascons"—have been an enduring puzzle to lunar scientists since they were first observed during analysis of the Lunar Orbiter mission [1]. The data returned by NASA's Gravity Recovery and Interior Laboratory (GRAIL) mission [2] have enabled highly detailed characterization of these anomalies, allowing new and more detailed models to be made of the origin of these striking features.

The multi-ringed Orientale basin (19.4 °S, 267.2 °E) has a gravity signature most similar to that of other lunar mascons that are largely devoid of volcanic fill, though the same basic pattern exists even in the mascons of the large nearside mare basins [2]. The pattern is that of a bulls-eye: a central positive free-air anomaly, a surrounding annulus with negative anomaly, and a distal annulus with a positive anomaly (Fig. 1a). In Orientale, the anomalies range from ~700 mGal negative to ~400 mGal positive (1 mGal = 10^{-5} m s^{-2}).

With a diameter of ~960 km, the Orientale basin is substantially larger than those considered in similar studies by Freed et al. [3] and Johnson et al. [4], spanning almost 30° of arc and potentially making the effects of surface curvature important [5]. Additionally, the center of the basin holds a mare unit ~250 km in diameter and ~200 m thick [6], giving it a central volcanic load that is present but much smaller than that of other nearside mascon basins, e.g., Humorum. Here we attempt to explain the origin and evolution of the mascon in Orientale Basin, and particularly to consider the above characteristics that differentiate it from other mascon basins on the Moon.

Methods: Our approach is a self-consistent combination of modeling techniques that allows us to explain the evolution of a basin from the time of impact through its long-term geophysical evolution. We first use a hydrocode, iSALE [e.g., 7,8], to simulate the time period from impact through crater collapse (spanning a few hours). These models are constrained by the location of the annulus of negative gravity anomaly at ~300 km radius, which is taken to correspond to a region of thickened crust [9,10], and by a regional ~40 km crustal thickness inferred from GRAIL data [11]; the size of the impactor and the thermal gradient of the Moon at time of impact are treated as variables.

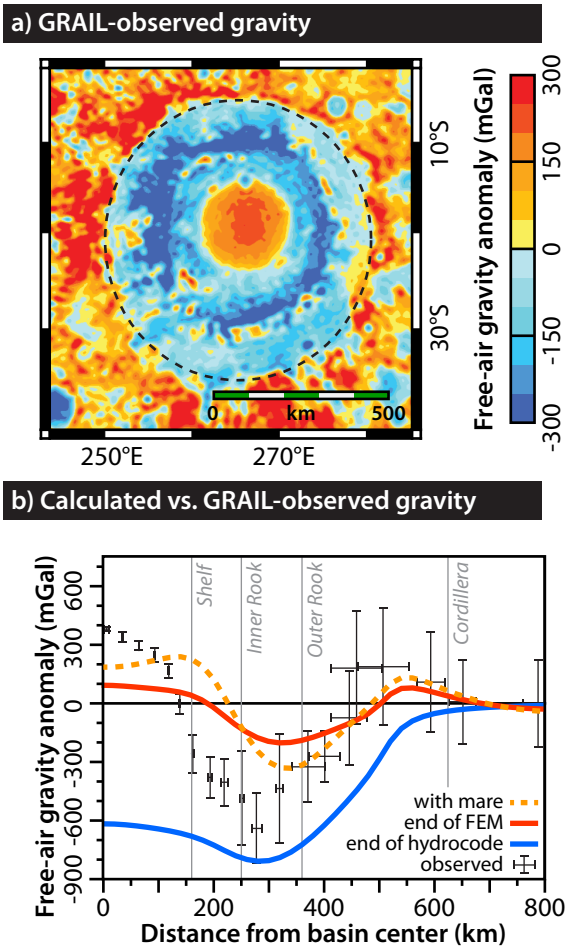

Figure 1. (a) Observed free-air gravity anomaly over Orientale basin, from a spherical harmonic expansion of GRAIL data to degree and order 420. **(b)** Preliminary models of the anomaly in the basin shortly after impact (blue line, taken from the start of the finite element simulation), after thermal and isostatic evolution of the basin (red line, taken from the end of the finite element simulation), and after mare emplacement (orange line, from simple approximations) as well as the observed free-air anomaly (crosses), plotted against distance from the center of the central positive anomaly. Horizontal error bars in observed data show the axial asymmetry of the basin, as azimuthal averaging was performed of major features of the free-air anomaly map (e.g., dashed line in Fig. 1a). The multiple basin rings (grey lines with captions) are one possible source of discrepancy between models and observations; this question remains to be explored.

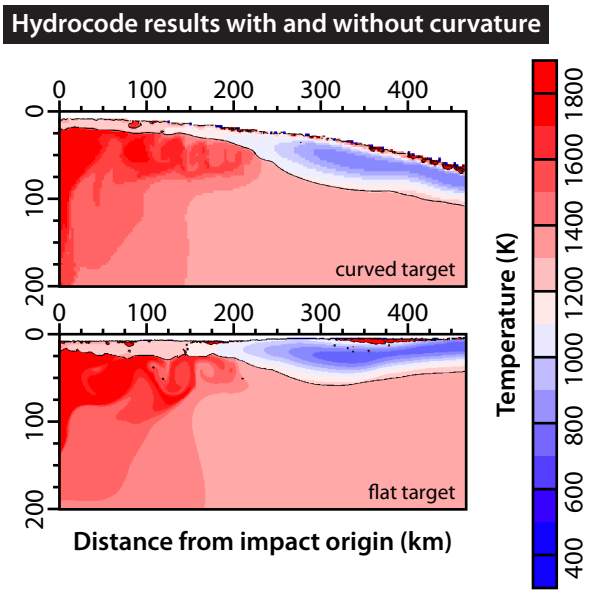

Figure 2. (top) The result of a hydrocode model of a 70 km dunite bolide impacting a spherical target at 15 km s^{-1}, ~2 hours after impact. Target consists of a 40-km-thick gabbroic crust overlying a dunite mantle. Model resolution is 2.5 km per cell. **(bottom)** Results for impact into a flat target, with the impactor and the target having the same properties described above. Here, model resolution is 1 km per cell.

The end state of the hydrocode model, after crater collapse, is then used as the starting condition for an axisymmetric finite element model (FEM), taking into account geometry, temperature, and density. The FEM then simulates the contraction of the melt pool and the isostatic relaxation of the basin, which is driven by a subsurface pressure gradient that drives mantle material inward toward the basin center. These two processes are linked in our models by the use of pressure- and temperature-dependent viscosity and density structure. After completion of the FEM, we calculate the gravity field of the model and subtract that of an undisturbed flat-layered model (representing the geoid) to arrive at a synthetic free-air gravity anomaly.

Results: We ran several models to test the importance of surface curvature on our simulations, as incorporating curved basin geometry in Abaqus requires the models to be run in three dimensions, incurring a substantial increase in time and computer resources. Hydrocode models of an impact into a curved basin show results with excavation cavity sizes and melt pool dimensions similar to simulations of impacts into a flat basin (Fig. 2). Flat and curved viscoelastic FEMs of a simplified geometry consisting of a 40 km crust with an annular thickened collar also show values for surface uplift above the center of the collar within 6% of one another. Because the differences between the two models were minimal in these simple test cases, we carried out all of the models of Orientale discussed below with flat axisymmetry.

A 70 km bolide impacting at 15 km s^{-1} into a Moon with a near-surface thermal gradient of 30 K km^{-1} provided the best match to the observed excavation diameter (~200 km [e.g. 10,12]) and the location of the annulus of thickened crust. The annulus is formed by the ejection of crustal material onto the periphery of the transient crater. This annulus then moves back inward toward the basin center, leaving a sub-isostatic configuration because of its frictional strength. The impact leaves a melt pool ~160 km in radius that extends to a depth of ~230 km under the center of the basin; the melt pool is capped at the surface by ~10–20 km of unmelted crust that flowed back over the pool during crater collapse.

Our FEM results are preliminary, as at the time of this writing we have not yet extensively explored model parameter space. Our results capture the general bulls-eye pattern of free-air anomaly observed in Orientale basin, although we currently underpredict the magnitude of both the mascon and the surrounding negative anomaly by ~200 mGal (Fig. 1b). This discrepancy may be due to the presence of the Inner Rook and shelf rings, which are likely to be faults [e.g. 13] not considered in the models; to a misestimation of crustal thickness at the center of the basin; or to density or viscosity structures other than those we have currently considered to date. All of these possible sources of error remain to be explored in our modeling.

The addition of mare to the basin improves the fit substantially. Although our results are preliminary, simple models indicate that the mare raises the free-air anomaly by ~90 mGal at the center of the basin and lowers it in the surrounding annulus by > 100 mGal. In our current models, however, flexure due to mare emplacement lowers the contribution at the very center of the basin (Fig. 1); this prediction does not match observations and warrants further investigation in our models. These figures are consistent with previous estimates of the mare contribution [e.g. 14]

References: [1] Sjogren, W. L., and Muller P. M. (1968) *Science* 161, 680. [2] Zuber, M. T. et al. (2012) *Science*, doi:10.1126/science.1231507. [3] Freed, A. M. et al. (2013) *LPSC* 44. [4] Johnson, B. et al. (2013) *LPSC* 44. [5] Freed, A. M. et al. (2001) *JGR* 106, E9. [6] Whitten, J. et al. (2011) *JGR* 116, E00G09. [7] Amsden, A. A. et al. (1980) *LANL Rep. LA-8095*, 101. [8] Wünnemann, K. et al. (2006) *Icarus* 180, 514. [9] Neumann, G. A. et al. (1996) *JGR* 101, E7. [10] Wieczorek, M. A., and Phillips, R. J. (1999) *Icarus* 139, 246. [11] Wieczorek, M. A. et al. (2012) *Science* 10.1126/science.1231530. [12] Spudis, P. D. et al. (1984) *LPSC* 15, *JGR* 89, C197. [13] Head, J. W. (1974), *The Moon* 11, 327. [14] Andrews-Hanna, J. C. (2012) *LPSC* 43, 2804.